3113

LA-UR-03-xxxx
Approved for public release;
distribution is unlimited.

May 1, 2003

c 1

Title: Pore Collapse and Hot Spots in HMX

Author(s): RALPH MENIKOFF

Submitted to: APS Topical Conference
Shock Compression of Condensed Matter
Portland, Oregon
July 20–25, 2003

45

PORE COLLAPSE AND HOT SPOTS IN HMX

Ralph Menikoff

Theoretical Division, MS-B214, Los Alamos National Laboratory, Los Alamos, NM 87545

Abstract. The computing power now available has led researchers to reconsider mesoscale simulations as a means to develop a detailed understanding of detonation waves in a heterogeneous explosive. Since chemical reaction rates are sensitive to temperature, hot spots are of critical importance for initiation. In a plastic-bonded explosive, shock desensitization experiments imply that hot spots generated by pore collapse dominate shock initiation. Here, for the collapse of a single pore driven by a shock, the dependence of the temperature distribution on numerical resolution and dissipative mechanism is investigated. An inert material (with the constitutive properties of HMX) is used to better focus on the mechanics of pore collapse. Two important findings resulted from this study. First, too low a resolution can significantly enhance the hot-spot mass. Second, at even moderate piston velocities (< 1 km/s), shock dissipation alone does not generate sufficient hot-spot mass. Two other dissipative mechanism investigated are plastic work and viscous heating. In the cases studied, the integrated temperature distribution has a power-law tail with exponent related to a parameter with dimensions of viscosity. For a particular case, the parameter of either dissipative mechanism can be fit to obtain quantitatively the hot-spot mass needed for initiation. But the dissipative mechanisms scale differently with shock strength and pore size. Consequently, to predict initiation behavior over a range of stimuli and as the micro-structure properties of a PBX are varied, sufficient numerical resolution and the correct physical dissipative mechanism are essential.

INTRODUCTION

It has been known since the 1950's that initiation in a plastic-bonded explosive (PBX) is due to thermal reactions but require hot spots (1). Hot spots reconcile the large discrepancy between the time to detonation from Pop plot data and the adiabatic induction time based on the bulk shock temperature and an Arrhenius reaction rate, see figure 1. For a strong shock ($P = 10\,\text{GPa}$) at the high end of the measured Pop plot in HMX based PBX-9501, we note that the time to detonation is $\simeq 0.2\,\mu\text{s}$. Fast reaction on this time scale (20 ns) require temperatures in range of 800 K for the liquid phase (9) to 1500 K for the solid phase (6), see figure 2.

Shock desensitization experiments (2) and the increased sensitivity of a PBX with increasing porosity, as displayed in Pop plot data, imply that hot spots generated by pore collapse dominate a shock-to-detonation transition. Early hydrodynamic simulations of heterogeneous initiation by Mader (8, sec. 3.3) utilized artificial viscosity for shock waves as the only dissipative mechanism. They showed that a micro-jet is formed when a strong shock impinges on a pore, and then a hot spot is produced when the jet impacts the downstream side of the pore. Furthermore, Mader's simulations with arrays of pores in an explosive showed a shock-to-detonation transition. When the simulations were performed (2-D flow in the 1960s and 3-D in the 1980's), the available computer power limited the resolution. In addition, data on the thermal properties of explosives were limited. The variation of specific heat with temperature is important because of the sensitivity of reaction rates.

With only shock dissipation, the peak pore collapse temperature can be estimated based solely on the equation of state (EOS) of the explosive and simple Riemann problems. For beta-HMX, which is the stable polymorph at ambient conditions, a complete EOS is derived from data currently available and estimates of the hot-spot temperature have been

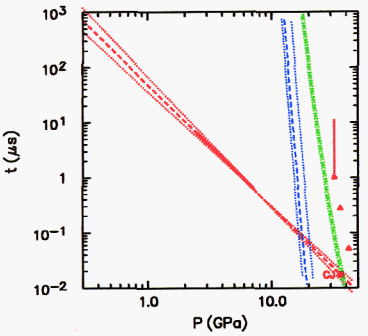

FIGURE 1. Time to detonation as function of shock pressure for HMX. Red line is Pop plot for PBX-9501 (4). Blue and green lines are adiabatic induction time for Arrhenius reaction rate based on liquid HMX (9) and "global reaction rate" (6), respectively. Symbols are from wedge experiments of single crystal HMX by Craig (2).

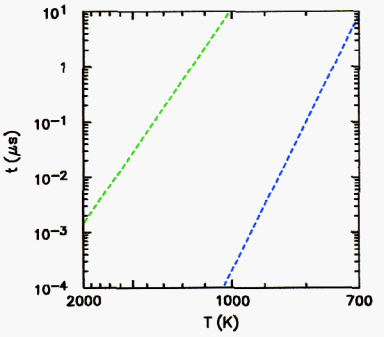

FIGURE 2. Adiabatic induction time for HMX. Blue and green lines are based on Arrhenius reaction rate for liquid HMX (9) and "global reaction rate" (6), respectively.

presented (10). Since the EOS neglects solid-liquid phase transition, which has a latent heat equivalent to $\Delta T \simeq 200\,\mathrm{K}$, we take T=1000 K as critical hot-spot temperature for fast reaction. The estimates indicate that shock dissipation alone does not generate sufficiently high hot-spot temperatures, even for a strong shock at the high end of the measured Pop plot.

Other dissipative mechanism applicable to pore collapse are viscous heating and plastic work. In the past, hot-spot temperatures were estimated based on simplified models due to the limited computer power available at the time, see for example (7, 3). Here, for the collapse of a single pore driven by a shock, the dependence of the temperature distribution on numerical resolution and dissipative mechanism is investigated.

We consider both shear viscosity and rate-dependent plasticity. These mechanisms introduce a parameter η with dimensions of dynamic viscosity. For plasticity the parameter determines the relaxation rate to the yield surface. The viscous parameter give rise to two dimensionless parameters: Reynolds number, $Ry = \frac{\rho u R}{\eta}$ and (shock width)/(pore radius). Consequently, scaling of hot-spot temperature with pore radius and particle velocity will depend on the dissipative mechanism. To study this dependence we choose to hold the pore radius fixed and vary the viscosity parameter.

SIMULATIONS

Initial conditions for two-dimensional simulations are a gas filled pore of radius 0.1 mm centered at (0.4,0) mm surrounded by an inert material with the mechanical properties of HMX. The left boundary is a piston. A piston velocity of 1.3 km/s is used to drive a shock wave with a pressure of 13 GPa and temperature of 630 K.

For hydrodynamic pore collapse, in which the only dissipation is at shock fronts, figure 3A shows the temperature field after the shock front has passed over the pore. We note that the gray region corresponds to the piston and the blue region to the gas. Pore collapse gives rise to an outgoing rarefaction wave in the material compressed by the lead shock, followed by an outgoing shock wave. These secondary waves give rise to the main features seen in the temperature field. We note that the secondary shock has caught up to the lead shock resulting in a Mach wave pattern. The temperature discontinuity corresponds to the contact emanating from the Mach triple point at (0.82,0.14). The gas pore has been highly compressed and distorted by the vortex set up from the impact of the micro-jet, formed when the lead shock overtakes the pore, on the downstream side of the pore. Since the vortex and the gas interface are expected to be unstable, the shape of the pore are undoubtedly inaccurate.

The temperature distribution is shown in figure 3B. The first peak at 300 K corresponds to the ambient state ahead of the lead shock front. The second peak centered at 575 K (greenish region) corre-

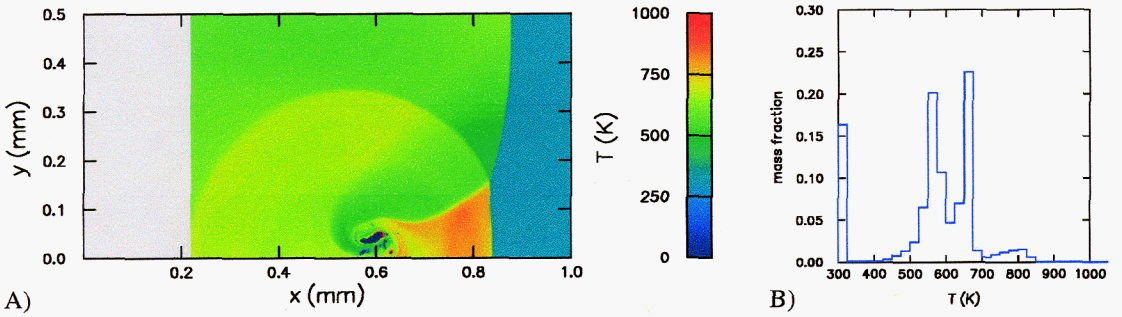

FIGURE 3. Temperature after pore collapse. Simulation with piston velocity of 1.3 km/s, shock dissipation only and resolution of 100 cells in the initial pore radius (0.1 mm). A) 2-D temperature field, gray region is piston and blue region is gas pore. Bottom boundary is symmetry plane. B) Temperature distribution.

sponds to the material heated by the lead shock and then cooled by the rarefaction from the pore implosion. The third peak centered about 675 K (yellow-red region) corresponds to the material heated by the lead shock and backward expanding portion of the secondary shock from the explosion of the pore. The low broad peak between 700 and 850 K (red region) corresponds to the region between the Mach stem and the material directly impacted by the micro-jet. The highest HMX temperatures, above 850 K, occur only near the pore and are numerical artifacts of the material interface treatment.

We note that the third peak is similar to what Hayes (5, Fig. 5) used to model initiation in HNS. The temperature of this peak depends on the explosive through its equation of state and specific heat. For HMX, since 1000 K is needed for fast reactions, we conclude that shock dissipation is not sufficient for initiation.

With additional dissipative mechanisms, plastic work or viscous heating, the tail of the temperature distribution can be greatly enhanced. Consequently, the reaction from hot spots are associated with the extreme tail of the temperature distribution. The tail of the temperature distribution is best described by the integrated temperature distribution, mass(T_1) at $T > T_1$. The mass is normalize relative to the equivalent mass in the pore volume at the initial explosive density.

Before reporting the results of simulations with other dissipative mechanisms we examine the effect of mesh resolution on the temperature distribution. Figure 4 shows the integrated temperature distribution for resolution varying from 5 to 100 cells in the initial pore radius. We note that the distributions are nearly the same up to 800 K, but differ substantially in the high temperature tail. The differences are largely due to truncation errors in the region of high vorticity around the pore. In fact the low resolution case has sufficient hot-spot mass above 1000 K that if the simulation included chemical reaction a substantial amount of burn would occur, roughly a burn mass equivalent to 25% of the volume of the pore. Thus, errors from too low a resolution can substantially affect simulations of initiation. This is an important concern for meso-scale simulations of hot-spot initiation and is a determining factor in the size or number of grains in a PBX that can be included in the computational domain.

Simulations with additional dissipative mechanisms are summarized by the integrated temperature distribution shown in figure 5. A striking feature of the integrated distributions are that they are approximately linear on a log-log scale. This implies that the tail of the distribution has a power-law behavior. Moreover, the slope of the temperature distribution or the exponent of the power-law increases with the viscous parameter. The viscous parameter has not been directly measured. Instead it is usual fit to reproduce integral data in a limited class of experiments. The fact that both the viscous heating and plastic work have similar distributions implies that either dissipative mechanism can be used in a fit. To distinguish these mechanism requires a range of ex-

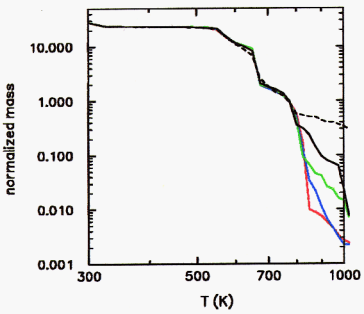

FIGURE 4. Variation of temperature distribution with resolution for shock dissipation only. Cells in pore radius: red, 100; blue, 50; green, 20; black, solid and dashed 10 and 5, respectively.

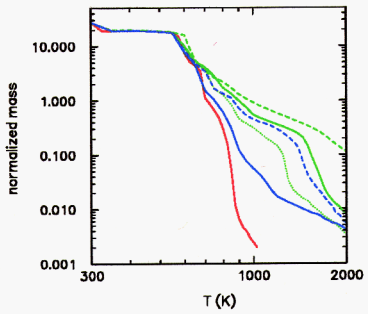

FIGURE 5. Variation of temperature distribution with dissipative mechanism. Dissipative mechanisms: red, shock heating; blue, shear viscosity, solid and dashed $\eta = 10$ and 100 Poise, respectively; green, rate dependent plasticity, solid, dashed and dotted $\eta = 800$, 8000 and 80 Poise, respectively.

periments which are sensitive to differences in the scaling behavior of each mechanism.

CONCLUSIONS

Two important findings resulted from this study. First, too low a resolution can significantly enhance the hot-spot mass. Second, at even modest piston velocities (< 1 km/s), shock dissipation alone does not generate sufficient hot-spot mass. Two other dissipative mechanism investigated are plastic work and viscous heating. In the cases studied, the integrated temperature distribution has a power-law tail with exponent related to a parameter with dimensions of viscosity. The dissipative mechanisms scale differently with shock strength and pore size. Consequently, to predict initiation behavior over a range of stimuli and as the micro-structure properties of a PBX are varied, sufficient numerical resolution and the correct physical dissipative mechanism are essential.

ACKNOWLEDGMENTS

This work was carried out under the auspices of the U. S. Dept. of Energy at LANL under contract W-7405-ENG-36. The author thanks Prof. David Benson, Univ. of Calif. at San Diego, for providing the code used for the simulations.

REFERENCES

1. Bowden, F. P., and Yoffe, Y. D., *Initiation and Growth of Explosion in Liquids and Solids*, Cambridge Univ. Press, Cambridge, UK, 1952.
2. Campbell, A. W., and Travis, J. R., in *Proceedings of Eighth Symposium (International) on Detonation, Albuquerque, NM, July 15–19, 1985*, Naval Surface Weapons Center, White Oak, Silver Spring, Maryland 20903–5000, 1986 pp. 1057–1068.
3. Frey, R. B., in *Eighth Symposium (International) on Detonation*, 1985 pp. 68–80.
4. Gibbs, T. R., and Popalato, A., eds., *LASL Explosive Property Data*, University of California Press, 1980.
5. Hayes, D. B., in *Progress in Astronautics and Aeronautics*, vol. 87, 1983 pp. 445–467.
6. Henson, B. F., Asay, B. W., Smilowitz, L. B., and Dickson, P. M., Ignition chemistry in HMX from thermal explosion to detonation, Tech. Rep. LA-UR-01-3499, Los Alamos National Lab., 2001.
7. Khasainov, B. A., Attetkov, A. V., Borisov, A. A., Ermolaev, B. S., and Soloviev, V. S., in *Progress in Astronautics and Aeronautics*, vol. 114, 1988 pp. 303–321.
8. Mader, C. L., *Numerical Modeling of Explosives and Propellants*, second edn., CRC Press, Baca Raton, FL, 1998.
9. Rogers, R. N., *Thermochimica Acta* **11**, (1975) 131–139.
10. Sewell, T. D., and Menikoff, R., in *Shock Compression of Condensed Matter*, 2003 p. this volume.